JOURNAL OF Materials CHEMISTRY

# Influence of the composition of a $H_2$–$CH_4$ gas mixture on the catalytic synthesis of carbon nanotubes–Fe/$Fe_3C$–$Al_2O_3$ nanocomposite powders

**A. Peigney, Ch. Laurent and A. Rousset**

*Laboratoire de Chimie des Matériaux Inorganiques, ESA CNRS 5070, Université Paul-Sabatier, 31062 Toulouse cedex 4, France. E-mail: peigney@iris.ups-tlse.fr*

***Received 23rd November 1998, Accepted 1st March 1999***

$C_{NTs}$–Fe/$Fe_3C$–$Al_2O_3$ nanocomposite powders have been prepared by selective reduction of an α-$Al_{1.9}Fe_{0.1}O_3$ solid solution in $H_2$–$CH_4$ gas mixtures (0, 1.5, 3, 4.5, 6, 9, 12, 14, 16, 18, 24, 30 and 45 mol% $CH_4$). The powders have been studied using macroscopic and microscopic techniques. The $C_{NTs}$ are arranged in very long bundles homogeneously dispersed in the composite powder. Most $C_{NTs}$ have less than four walls and are free of pyrolytic or amorphous carbon deposits. The inner diameter is in the range 1–6 nm, which could indicate that the catalyst particles active for $C_{NTs}$ formation are in this size range. The reduction of the $Fe^{3+}$ ions to metallic Fe is highly favoured by the presence of $CH_4$ in the reduction atmosphere. There are more $Fe_3C$ than α-Fe particles located at the surface of the matrix grains for $CH_4$ contents higher than 4.5 mol%, however, the exact nature of the catalytically active particles remains an open question. Compositions in the range 9–18 mol% $CH_4$ give the best results.

## Introduction

A worldwide research effort on carbon nanotubes ($C_{NTs}$) is currently taking place. This was prompted by Iijima's report[1] on the obtention of carbon tubes with a diameter in the nanometer range and on their relations with fullerenes. Indeed, albeit $C_{NTs}$ present some characteristics similar to those of hollow carbon fibres, which are known for several decades, both their nanometric diameter and particular structure lead to truly unique properties. Notably, $C_{NTs}$ are materials with extraordinary strength and flexibility which resist failure under repeated bending.[2–8] Thus, they are considered as the ultimate carbon fibres and are potentially attractive materials as reinforcing elements in composites.[9–11]

The synthesis methods of $C_{NTs}$ have been reviewed by Journet and Bernier.[12] Most are based on the sublimation of carbon in an inert atmosphere, such as the electric-arc-discharge process, laser ablation or sublimation by solar energy, but chemical methods such as catalytic decomposition of hydrocarbons, electrolysis in a molten ionic salt, heat-treatment of polymers, low-temperature solid pyrolysis and *in situ* catalysis are also used. Several of these methods involve the use of nanometric metal particles. Laurent *et al.*[13] have recently reviewed the various mechanisms proposed for nanotube nucleation and growth from such particles and the micro/nanostructure of the materials obtained by different methods. The chemical methods are promising owing to ready availability of starting materials and low cost. Particularly, catalytic decomposition of hydrocarbons on metal particles (Fe, Co, Ni) leads to Iijima-type $C_{NTs}$ when the catalyst particles are sufficiently small. However, the main difficulty is to obtain nanometric particles, *i.e.* active particles, at the relatively high temperature (usually $>800\,^{\circ}C$) required for the formation of $C_{NTs}$ by catalytic decomposition of hydrocarbons. Ivanov *et al.*[14] and Hernadi *et al.*[15] used a zeolite-supported Co catalyst and obtained $C_{NTs}$ only 4 nm in diameter as well as 60 μm long tubes, but they point out that the longest tubes are also the thickest.

Our group has proposed an original catalytic method based on the selective reduction of oxide solid solutions.[16] Indeed, when using a $H_2$–$CH_4$ gas mixture for the reduction of an α-$Al_{1.9}Fe_{0.1}O_3$ solid solution, the pristine Fe nanoparticles formed *in situ* upon reduction were found to be active at a size suitable for the catalytic formation of carbon nanotubes. The so-obtained $C_{NTs}$–Fe–$Al_2O_3$ composite powders contain a large amount of single- and multi-walled $C_{NTs}$ with an outer diameter in the range 1.5–15 nm. The $C_{NTs}$ are mostly arranged in bundles smaller than 100 nm in diameter which may be up to 100 μm long. The total bundle length in 1 g of composite powder has been calculated to be $>100\,000$ km. These powders in which the $C_{NTs}$ bundles are very homogeneously dispersed between the metal oxide grains are interesting materials to prepare dense ceramic–matrix nanocomposites that include $C_{NTs}$.[17] In addition to electron microscopy characterisations, an original method using chemical analysis and specific surface area measurements has been developed[16,18] in order to characterize the composites at a macroscopic scale and thus produce data which are more representative of the material than those derived from local techniques. Two parameters representing the quantity of $C_{NTs}$ and the quality of the deposited carbon are calculated, a higher quality parameter indicating more carbon in tubular form and/or a smaller average tube diameter and/or tubes with fewer walls. This method was applied for various studies as summarized below. It was found necessary to use a stable α-$Al_{1.8}Fe_{0.2}O_3$ solid solution rather than amorphous- or η-$Al_{1.8}Fe_{0.2}O_3$ compounds as starting material in order to obtain carbon essentially in the form of nanotubes.[18] Indeed, in the latter cases, large quantities of non-tubular carbon are produced and some carbon is entrapped within the oxide grains upon their crystallization. Work using α-$Al_{2-2x}Fe_{2x}O_3$ ($0.02 \leqslant x \leqslant 0.20$) solid solutions as starting compounds[19] has shown that it is beneficial to reduce monophase oxide solid solutions ($x \leqslant 0.10$) rather than mixtures of $Al_2O_3$- and $Fe_2O_3$-rich solid solutions ($x > 0.10$) in order to favour the formation of $C_{NTs}$. The highest quantity of $C_{NTs}$ was obtained using α-$Al_{1.8}Fe_{0.2}O_3$ as starting compound, *i.e.* the product with the maximum Fe concentration allowing to retain monophase solid solution. By contrast, the higher carbon quality was obtained with only 5% Fe (α-$Al_{1.9}Fe_{0.1}O_3$) because the surface Fe nanoparticles formed upon reduction are probably slightly smaller, being less numerous and therefore less prone to coalescence, than those formed from α-$Al_{1.8}Fe_{0.2}O_3$. An increase of the reduction temperature from 900 to 1000 °C was found to produce an increase in the amount

of nanotubes[18,19] because the $CH_4$ sursaturation level in the reducing atmosphere is higher at 1000 than at 900 °C.[20] However, a simultaneous decrease in carbon quality indicated that a higher reduction temperature also favours tube thickening and/or the deposition of non-tubular carbon species. The formation of $C_{NTs}$–Fe/Co/Ni–$MgAl_2O_4$ composite powders has also been investigated.[21,22]

Obviously, the $CH_4$ content in the $H_2$–$CH_4$ gas mixture is an important parameter which can affect the formation of the Iijima-type $C_{NTs}$ in different ways. Firstly, comparison of the results of studies performed using either pure $H_2$[23] or an $H_2$–$CH_4$ atmosphere with 6 mol% $CH_4$[18] has indicated that the presence of $CH_4$ in the reducing gas mixture markedly favours the reduction of iron(III) ions substituting for aluminium in the corundum lattice. This may have consequences on the quantity and size of the catalyst nanoparticles formed at the surface of the matrix grains, and thus on the quantity and diameter of the $C_{NTs}$ formed from these nanoparticles. Secondly, the $CH_4$ concentration in the $H_2$–$CH_4$ mixture may modify the balance between the formation of pure Fe particles, Fe–C alloy particles and $Fe_3C$ particles, which in consequence may affect the nucleation and growth of the nanotubes. Lastly, the atmosphere composition may have an effect on the $CH_4$ decomposition pattern, which may also influence the deposition of carbon as $C_{NTs}$ or as undesirable forms such as thick fibers, thick and short tubes, thick graphene layers around the Fe particles, clusters of graphitic nanoparticles or amorphous deposits.

Several groups[24–26] have reported on the formation of carbon filaments or nanofibers in $H_2$–$CH_4$ atmosphere but there is no systematic study of the influence of its composition. In addition, the mechanisms responsible for Iijima-type $C_{NTs}$ formation could be distinct to those occurring in the case of filaments and nanofibers. Cui *et al.*[27] have used a 90 mol% $CH_4$ $H_2$–$CH_4$ gas mixture to prepare $C_{NTs}$ using Ni particles as catalyst. These authors obtained solid carbon fibers when performing the heat-treatment at 500 °C but obtained mainly $C_{NTs}$ when the experiment was carried out at 600 °C. Increasing the temperature to 700 °C resulted in the formation of fewer carbon species. They concluded that the temperature has to be high enough for the $H_2$ to maintain the catalyst particles in a reduced state but not too high to avoid the elimination of carbon species. Hernadi *et al.*[28] passed pure $CH_4$ over Fe–$SiO_2$ catalyst at 700, 750 and 800 °C and reported that the carbon yield is zero whatever the temperature. In contrast, Kong *et al.*[29] have reported the synthesis of single-walled $C_{NTs}$ by chemical vapor deposition of pure $CH_4$ on impregnated $Fe_2O_3/Al_2O_3$ catalyst. However, these authors used a very low catalyst loading (0.6 mmol $Fe_2O_3$/1 g $Al_2O_3$) and they furthermore pointed out that a quantitative measure of the $C_{NTs}$ yield in their materials is lacking.

The aim of this work is to study the influence of the $CH_4$ content in the $H_2$–$CH_4$ gas mixture on the synthesis of $C_{NTs}$–Fe–$Al_2O_3$ nanocomposite powders *via in situ* catalysis.[16] The stable, monophase, $\alpha$-$Al_{1.9}Fe_{0.1}O_3$ solid solution, which has previously given best results in terms of carbon quality,[18,19] is used as starting compound.

## Experimental

A powder of $\alpha$-$Al_{1.9}Fe_{0.1}O_3$ solid solution was prepared by decomposition in air at 400 °C for 2 h and further calcination at 1100 °C for 2 h of the corresponding mixed oxalate as described elsewhere.[18,19,30] The powder is composed of 10–20 μm agglomerates of submicronic or nanometric primary grains[18,19] and its specific surface area $S_{ss}$ is equal to $(5.00 \pm 0.15)$ $m^2\ g^{-1}$. Parts of the solid solution were reduced in $H_2$–$CH_4$ gas mixtures of different composition (0, 1.5, 3, 4.5, 6, 9, 12, 14, 16, 18, 24, 30 and 45 mol% $CH_4$) for 1 h at 1050 °C, giving rise to the $C_{NTs}$–Fe/$Fe_3C$–$Al_2O_3$ powders. For the sake of brevity, the reduced powders will hereafter be noted R0, R1.5, R3, …, R45. The gas flow was dried on $P_2O_5$ and its composition was set up using mass flow controllers. The flow rate was fixed at 250 sccm. Both the reduction temperature and dwell time were chosen after a preliminary experiment showing that, in comparison with previous work,[18,19] a temperature increase from 1000 to 1050 °C is not detrimental to the $C_{NTs}$ quality provided the dwell time is reduced from 4 to 1 h. For comparison, pure $\alpha$-$Al_2O_3$ was also heat-treated in different $H_2$–$CH_4$ atmospheres (4.5, 12, 18 and 24 mol% $CH_4$).

The powders were studied using scanning and transmission electron microscopy (SEM and TEM), X-ray diffraction (XRD) using Cu-K$\alpha$ radiation ($\lambda = 0.15418$ nm) and $^{57}$Fe Mössbauer spectroscopy. The Mössbauer spectra were recorded at room temperature with a constant acceleration spectrometer using a 50 mCi $^{57}$Co (Rh) source; the spectrometer was calibrated by collecting at room temperature the spectrum of a standard Fe foil and the centre shift (CS) values quoted hereafter are with reference to this standard. Part of the reduced powders were oxidized in air at 900 °C in order to eliminate all the carbon, as required for the specific surface area study. The specific surface areas of the oxide solid solution powder ($S_{ss}$), of the powders obtained after reduction ($S_n$) and of the specimens oxidized at 900 °C ($S_{on}$) were measured by the BET method using $N_2$ adsorption at liquid $N_2$ temperature. We used a Micromeritics FlowSorb II 2300 apparatus that gives a specific surface area value from one point (*i.e.* one adsorbate pressure) which then requires calibration. We determined that the reproducibility of the results is in the range $\pm 3\%$. The carbon content was determined by flash combustion with an accuracy of $\pm 2\%$.

## Results and discussion

### X-Ray diffraction

The nanocomposite powders prepared by reduction of the $\alpha$-$Al_{1.9}Fe_{0.1}O_3$ solid solution in different $H_2$–$CH_4$ gas mixtures have been studied by XRD and some patterns are shown in Fig. 1. The corundum peaks, representing the major phase, account for $\alpha$-$Al_2O_3$ or a partially reduced $\alpha$-$Al_{2-2y}Fe_{2y}O_3$ ($y \leqslant 0.05$) solid solution. The $\alpha$-Fe (110) peak ($d_{110} = 0.203$ nm) is detected in all the powders and is relatively wide except on the patterns of R0, R1.5 and R45. Since $Fe_3C$ obviously is not present in R0, the peak widening could reflect the formation of $Fe_3C$ particles, depending on the $CH_4$ content in the reducing atmosphere. Indeed, the most intense $Fe_3C$ peaks ($d_{210} = 0.206$ nm, $d_{022} = 0.202$ nm and $d_{121} = 0.210$ nm) could be present although they are not clearly resolved. $\gamma$-Fe may be present in all or some powders, but is extremely difficult to detect on the XRD patterns because the $\gamma$-Fe (111) diffraction peak ($d_{111} = 0.208$ nm) is probably masked by the corundum (113) base peak ($d_{113} = 0.209$ nm), the more so if $Fe_3C$ ($d_{121} = 0.210$ nm) is present as well. A shoulder on the high $2\theta$-side of the (102) corundum peak, which could correspond to the distance between graphene layers ($d_{002} = 0.34$ nm), is detected for R45. Since neither the ($hk0$) nor the other ($hkl$) reflexions, which would have much smaller intensities for nanotubes as well as for graphite are detected, it is not possible from this XRD pattern to discriminate between graphite and other graphenic forms of carbon such as nanotubes.

### $^{57}$Fe Mössbauer spectroscopy

All composite powders except R3 and R45 were studied by Mössbauer spectroscopy and typical spectra are shown in Fig. 2. Each spectrum was fitted assuming it is the sum of different subspectra : a doublet accounting for paramagnetic $Fe^{3+}$ ions substituting for $Al^{3+}$ ions in the $Al_2O_3$ lattice, a sextet accounting for ferromagnetic $\alpha$-Fe, a singlet character-

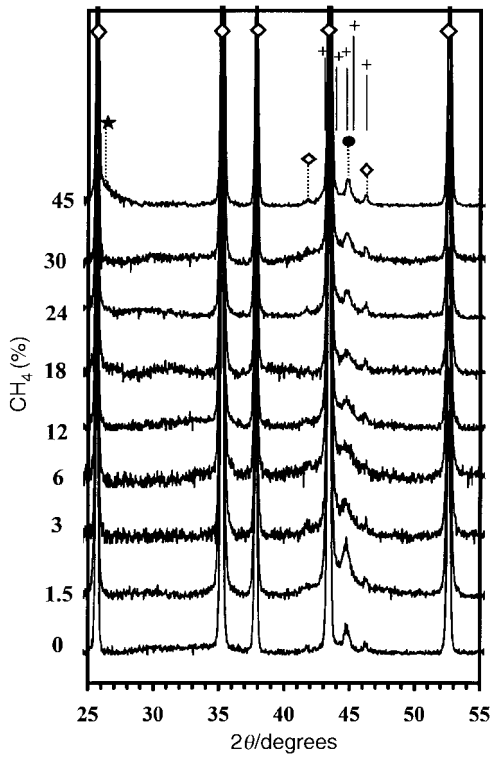


**Fig. 1** XRD patterns of nanocomposite powders prepared by reduction in $H_2$–$CH_4$ gas mixtures. The $CH_4$ content is indicated; (◇) $\alpha$-$Al_2O_3$, (●) $\alpha$-Fe, (★) corresponding to $d_{002}$ in multiwalled nanotubes and/or in graphite, (+) $Fe_3C$.

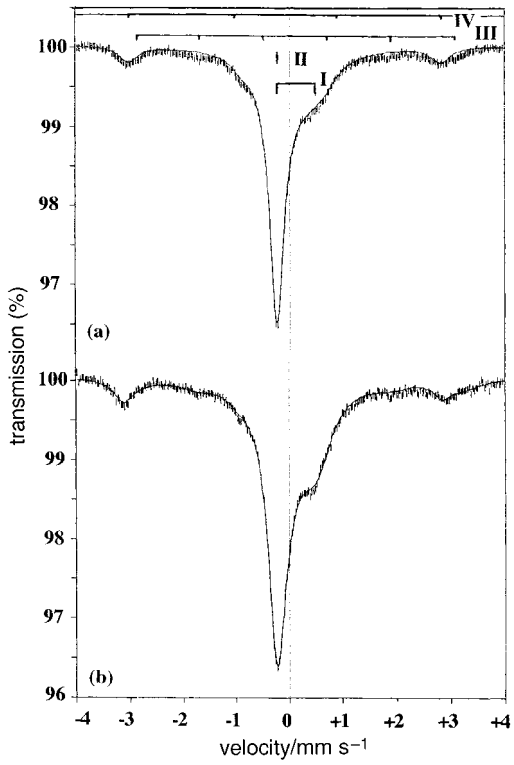


**Fig. 2** Typical room temperature $^{57}Fe$ Mössbauer spectra of the nanocomposite powders prepared by reduction in $H_2$–$CH_4$ gas mixtures contaning 4.5 mol% $CH_4$ (a) and 12 mol% $CH_4$ (b); I, paramagnetic $Fe^{3+}$ substituting in $\alpha$-$Al_2O_3$; II, non-ferromagnetic Fe; III, ferromagnetic $Fe_3C$; IV, ferromagnetic $\alpha$-Fe (the outer wings of the sextet are beyond the velocity range).

istic of non-ferromagnetic Fe and a sextet representing $Fe_3C$ (Table 1). Since $Fe_3C$ has two inequivalent Fe crystallographic sites,[31] the Mössbauer parameters of the sextet accounting for $Fe_3C$ correspond to the average of the two Fe-site parameters one may obtain using two sextets for the fit. Our average values are in good agreement with those reported by Le Caër *et al.*[32] for bulk $Fe_3C$ and by Bi *et al.*[33] for $Fe_3C$ nanoparticles. The hyperfine field is slightly lower but this may be a fit artefact arising because the present cementite particles are a minor phase in the composite powders. $Fe^{2+}$ ions were not detected in agreement with previous studies.[18,23]

The proportions of the different Fe species vary from one powder to another. Notably, the proportion of the $Fe^{3+}$ ions is decreased by a factor of two when using a 1.5 mol% $CH_4$ $H_2$–$CH_4$ atmosphere instead of pure $H_2$ [Fig. 3(a)], which confirms the earlier report[18] that the reduction of the $Fe^{3+}$ ions substituting for aluminium in the corundum lattice is markedly favoured by the presence of $CH_4$. However, the proportion of $Fe^{3+}$ ions slightly but steadily increases with an increase in $CH_4$ content from 1.5 to 30 mol%. Most interestingly, the evolution of the non-ferromagnetic Fe proportion is opposite to that of the $Fe^{3+}$ ions [Fig. 3(a)]. The proportions of the subspectra accounting for ferromagnetic $\alpha$-Fe and $Fe_3C$ are shown in [Fig. 3(b)], but no clear evolution can be observed, partly because of a relatively high uncertainty on their relative proportions. The trend is that there is more $Fe_3C$ than $\alpha$-Fe for $CH_4$ contents higher than 4.5 mol%. Whatever the $CH_4$ content, the sum of the proportions of the $Fe^{3+}$ ions and the non-ferromagnetic Fe represents *ca.* 74% of all the iron species and accordingly, the sum of the proportions of the two remaining subspectra, accounting for ferromagnetic $\alpha$-Fe and $Fe_3C$, represents *ca.* 26% of all the iron species [Fig. 3(c)].

It is proposed that, in a first approximation, the $\alpha$-Fe and $Fe_3C$ particles are formed by the reduction of the $Fe^{3+}$ ions which are located at and close to the surface of the oxide solid solution grains and thus are easily reducible at 1050 °C whatever the $CH_4$ content in the $H_2$–$CH_4$ mixture. The so-obtained particles are located at the surface of the matrix grains and could act as catalysts for the formation of the $C_{NTs}$. The hyperfine field of the sextet accounting for ferromagnetic $\alpha$-Fe was found to be lower than the accepted value for metallic iron (330 kG) for some composites (R4.5–R12), which could reflect the presence of carbon atoms neighbouring to iron atoms in the $\alpha$-Fe lattice.[34,35] It follows that, in a first approximation, the non-ferromagnetic Fe particles are mostly formed from the inner, less easily reducible $Fe^{3+}$ ions and therefore are located inside the alumina grains. Thus, it is probable that these particles are inactive for the formation of the $C_{NTs}$, in line with results presented in the following sections. The non-ferromagnetic phase of Fe could be either antiferromagnetic, paramagnetic or superparamagnetic $\alpha$-Fe or $\gamma$-Fe. Paramagnetic $\alpha$-Fe has been observed in Fe/Ni–$MgAl_2O_4$ nanocomposite powders[36] and superparamagnetic $\alpha$-Fe was found to be present in some Fe-$Al_2O_3$ specimens.[23,37,38] It is probable that the singlet represents superparamagnetic $\alpha$-Fe particles in the R0 specimen since the present experimental conditions for that powder are similar to those used for earlier studies.[23,37,38] This is in line with the slightly positive value observed for the IS (0.06 mm $s^{-1}$). However, the IS of the singlet for most of the other powders has a negative value, which points towards the face-centered-cubic $\gamma$-Fe phase. It has been hypothesized[18] that this could reflect the formation of a $\gamma$-Fe–C alloy, rather than pure Fe, but this is in contradiction with the present proposal that the particles are intragranular and therefore are probably protected from alloying with carbon. However, it is possible that a small proportion of the non-ferromagnetic particles are in fact located at the surface of the alumina grains, which could explain the slightly positive and negative deviations observed on the plots of the pro-

**Table 1** Room temperature Mössbauer parameters of some nanocomposite powders; para: paramagnetic; ferro: ferromagnetic; non-ferro: non-ferromagnetic; $\Delta E_Q$: quadrupole splitting/mm s$^{-1}$ $H$: hyperfine field/kG; IS: center shift/mm s$^{-1}$; $\Gamma$: halfline width/mm s$^{-1}$; P: proportion (%)

| | Para $Fe^{3+}$ | | | | Ferro α-Fe | | | | Non-ferro Fe | | | $Fe_3C$ | | | |
|---|---|---|---|---|---|---|---|---|---|---|---|---|---|---|---|
| Specimen | CS | $\Delta E_Q$ | $\Gamma$ | P | CS | $\Delta E_Q$ | $\Gamma$ | P | CS | $\Gamma$ | P | CS | $H$ | $\Gamma$ | P |
| R0 | 0.26 | 0.55 | 0.29 | 72 | −0.01 | 333 | 0.22 | 20 | 0.06 | 0.11 | 8 | — | — | — | 0 |
| R1.5 | 0.30 | 0.51 | 0.50 | 33 | 0.01 | 328 | 0.17 | 29[a] | −0.13 | 0.16 | 38 | — | — | — | —[a] |
| R4.4 | 0.24 | 0.61 | 0.52 | 38 | −0.03 | 321 | 0.20 | 16 | −0.13 | 0.16 | 37 | 0.20 | 191 | 0.31 | 9 |
| R6 | 0.26 | 0.61 | 0.42 | 36 | 0.01 | 324 | 0.15 | 9 | −0.13 | 0.16 | 34 | 0.16 | 188 | 0.49 | 21 |
| R9 | 0.28 | 0.60 | 0.46 | 41 | −0.04 | 324 | 0.16 | 11 | −0.12 | 0.17 | 32 | 0.21 | 195 | 0.40 | 16 |
| R12 | 0.30 | 0.55 | 0.36 | 40 | −0.03 | 311 | 0.19 | 14 | −0.11 | 0.29 | 33 | 0.20 | 189 | 0.39 | 13 |
| R14 | 0.27 | 0.62 | 0.36 | 45 | 0.01 | 330 | 0.12 | 8 | −0.11 | 0.19 | 29 | 0.14 | 190 | 0.45 | 18 |
| R16 | 0.27 | 0.59 | 0.37 | 50 | 0.00 | 329 | 0.14 | 11 | −0.10 | 0.19 | 29 | 0.21 | 196 | 0.40 | 10 |
| R18 | 0.27 | 0.61 | 0.34 | 48 | −0.02 | 330 | 0.15 | 7 | −0.01 | 0.20 | 25 | 0.16 | 191 | 0.47 | 20 |
| R24 | 0.26 | 0.62 | 0.32 | 54 | 0.01 | 332 | 0.15 | 10 | −0.05 | 0.21 | 23 | 0.19 | 195 | 0.40 | 13 |
| R30 | 0.23 | 0.66 | 0.28 | 60 | −0.01 | 329 | 0.11 | 9 | 0.02 | 0.17 | 16 | 0.20 | 203 | 0.40 | 15 |

[a]The proportion of ferromagnetic α-Fe is overestimated because there is probably a small proportion of $Fe_3C$ in this powder.

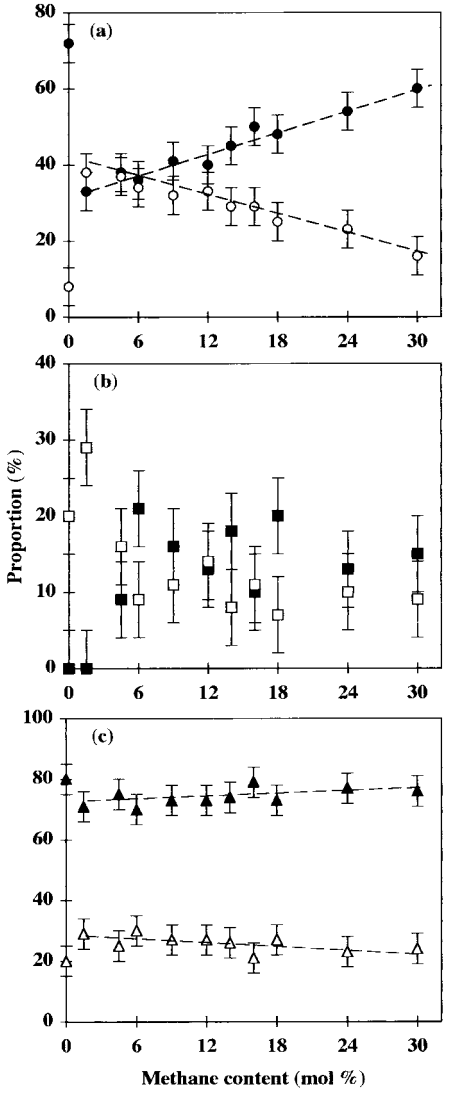


**Fig. 3** Proportions of the different iron species, as calculated from the Mössbauer spectra, *versus* the $CH_4$ content in the $H_2$–$CH_4$ reduction gas mixture. (a) paramagnetic $Fe^{3+}$ substituting in α-$Al_2O_3$ (●) and non-ferromagnetic Fe (○), (b) ferromagnetic α-Fe (□) and $Fe_3C$ (■), (c) the sum of the proportions of paramagnetic $Fe^{3+}$ and non-ferromagnetic Fe (▲) and the sum of the proportions of ferromagnetic α-Fe and $Fe_3C$ (△). Dotted lines are a guide to the eye.

portions of the intragranular and surface Fe species, respectively, *versus* the $CH_4$ content [Fig. 3(c)]. One may expect that the presence of $CH_4$ in the reduction atmosphere, which strongly favours the reduction of the $Fe^{3+}$ ions, favours the formation of these Fe particles at a relatively low temperature and that their size is thus small enough to suppress the γ–α transformation upon cooling from the reduction temperature. In addition, it should be noted that both γ-Fe and superparamagnetic α-Fe could be present in the same powder and that the parameters of the singlet could in fact be an average of those of the two corresponding singlets. This may account for the IS values found for the R18, R24 and R30 powders.

### Carbon content and specific surface area measurements

The carbon content measured in the nanocomposite powders [$C_n$, Table 2, Fig.4(a)] increases with the $CH_4$ content in the reducing gas mixture. However, the increase is attenuated between 6 and 12 mol% $CH_4$ as shown in an enlargement of the plot between 0 and 20 mol% $CH_4$ [Fig. 4(b)]. It is noteworthy that the gain in deposited carbon is considerable (from 6.71 to 17.92 wt%) when the $CH_4$ content is varied from 30 to 45 mol% $CH_4$.

The specific surface area of most nanocomposite powders ($S_n$, Table 2 and Fig. 5) is higher than the specific surface area of the starting solid solution [$(5.00\pm0.15)$ m$^2$ g$^{-1}$]. Taking into account the uncertainty, the $S_n$ values for R0 and R1.5 (4.92 and 4.84 m$^2$ g$^{-1}$, respectively) are not significantly different from 5.00 m$^2$ g$^{-1}$. For $CH_4$ contents higher than 1.5 mol%, $S_n$ almost linearly increases (up to 12.57 m$^2$ g$^{-1}$) when the $CH_4$ content is increased up to 24 mol%, but decreases for higher concentrations (30 and 45 mol% $CH_4$). As pointed out in earlier work,[16,18,19] it is the deposition of carbon in the composite powder, particularly in the form of $C_{NTs}$, which is responsible for most of this additional surface area. The Fe and/or $Fe_3C$ particles which form at the surface of the matrix grains can also contribute to this increase of surface area, but to a much smaller extent. After all the carbon is eliminated by air oxidation at 900 °C, the resulting specific surface areas [$(S_{on})_1$, Table 2 and Fig. 5] of powders R0–R18 can be considered as equal to $(S_{on})_2=(5.00\pm0.15)$ m$^2$ g$^{-1}$, *i.e.* the specific surface area of the starting solid solution. This latter value will be used for further calculations (Table 2). Since the reduction is performed at 1050 °C for 1 h, which is a milder treatment than the calcination step previously performed on the oxide solid solution (1100 °C, 2 h), it is a reasonable assumption that only very little sintering of the matrix grains occurs during the reduction thermal treatment. This confirms that the surface area corresponding to the iron oxide nanoparticles formed by oxidation of the iron and/or iron carbide particles dispersed at the surface of the matrix grains is either negligible or is masked by a slight sintering. However, for R30 and R45, and also possibly for R24, $(S_{on})_1$ is significantly lower than $(5.00\pm0.15)$ m$^2$ g$^{-1}$, which could indicate that a significant sintering of the matrix grains has taken place during the reduction when using $CH_4$-richer gas

**Table 2** Some characteristics of the powders containing carbon nanotubes: carbon content ($C_n$) and specific surface areas[a]

| $CH_4$ (mol%) | $C_n$ (wt%) | $S_n/m^2\ g^{-1}$ | $(S_{on})_1/m^2\ g^{-1}$ | $(S_{on})_2/m^2\ g^{-1}$ | $\Delta S/m^2\ g^{-1}$ | $\delta(\Delta S)/m^2\ g^{-1}$ | $(\Delta S/C_n)/m^2\ g^{-1}$ | $\delta(\Delta S/C_n)/m^2\ g^{-1}$ |
|---|---|---|---|---|---|---|---|---|
| 1.5 | 0.14 | 4.84 | 5.02 | 5.00 | — | — | — | — |
| 3 | 0.35 | 5.47 | 5.12 | 5.00 | 0.47 | 0.31 | 134 | 92 |
| 4.5 | 0.78 | 6.34 | 5.11 | 5.00 | 1.34 | 0.34 | 172 | 47 |
| 6 | 1.00 | 7.02 | 5.14 | 5.00 | 2.02 | 0.36 | 202 | 40 |
| 9 | 1.23 | 7.93 | 4.94 | 5.00 | 2.93 | 0.39 | 238 | 36 |
| 12 | 1.47 | 8.32 | 4.97 | 5.00 | 3.32 | 0.40 | 226 | 32 |
| 14 | 1.85 | 9.48 | 4.84 | 5.00 | 4.48 | 0.43 | 242 | 28 |
| 16 | 2.26 | 10.04 | 4.94 | 5.00 | 5.04 | 0.45 | 223 | 24 |
| 18 | 2.67 | 11.12 | 4.97 | 5.00 | 6.12 | 0.48 | 229 | 23 |
| 24 | 4.83 | 12.57 | 4.79 | 4.79 | 7.78 | 0.52 | 161 | 14 |
| 30 | 6.71 | 11.29 | 4.00 | 4.00 | 7.29 | 0.46 | 109 | 9 |
| 45 | 17.92 | 11.31 | 3.90 | 3.90 | 7.41 | 0.46 | 41 | 3 |

[a] $S_n$: value measured for the nanocomposite powders; $(S_{on})_1$: value measured for the powders oxidized at 900 °C; $(S_{on})_2$: value retained for the calculations; $\Delta S = S_n - (S_{on})_2$, representing the quantity of carbon nanotubes (see text); $\delta(\Delta S)$: uncertainty on $\Delta S$; $\Delta S/C_n$, representing the carbon quality (see text); $\delta(\Delta S/C_n)$: uncertainty on $\Delta S/C_n$.

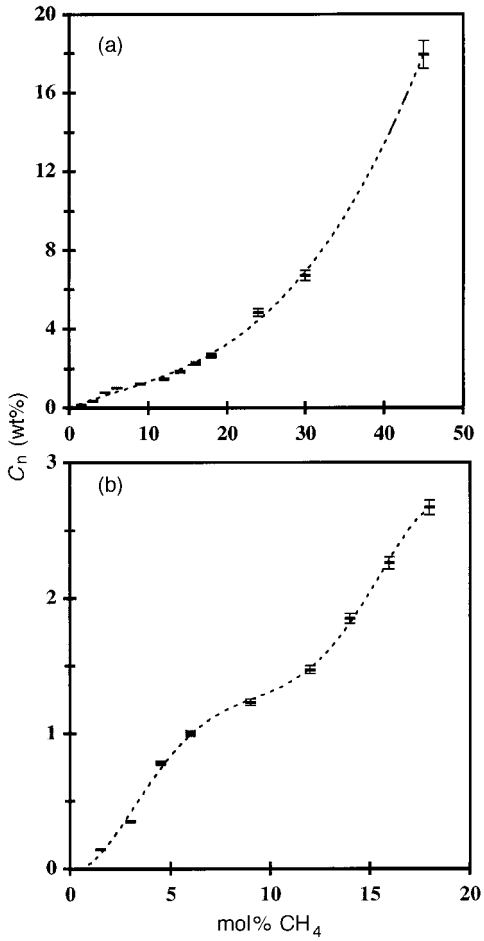


**Fig. 4** Carbon content ($C_n$) in the nanocomposite powders *versus* the $CH_4$ content (a) in the $H_2$–$CH_4$ reduction gas mixture and (b) enlargement showing the 0–18 mol% $CH_4$ range.

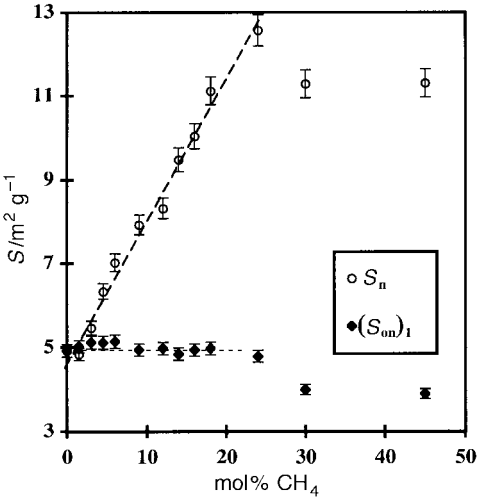


**Fig. 5** Specific surface area of the nanocomposite powders ($S_n$) and of the specimens oxidized in air at 900 °C [$(S_{on})_1$] *versus* the $CH_4$ content in the $H_2$–$CH_4$ reduction gas mixture.

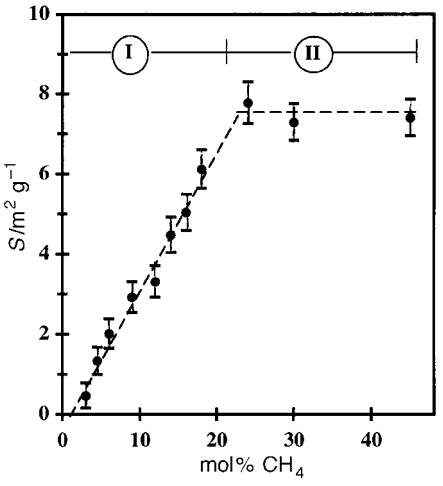


**Fig. 6** $\Delta S = S_n - (S_{on})_2$ *versus* the $CH_4$ content in the $H_2$–$CH_4$ reduction gas mixture.

mixtures. Thus, $(S_{on})_2$ values will be taken as equal to $(S_{on})_1$ values for powders R24, R30 and R45.

As proposed in previous work,[16,18] $\Delta S = S_n - (S_{on})_2$ represents the surface area of the carbon in the nanocomposite powder, which essentially corresponds to that of the $C_{NTs}$. Thus $\Delta S$ (Table 2, Fig. 6) reflects the quantity of $C_{NTs}$ (more precisely of nanotubes bundles) in the nanocomposite powder. Fig. 6 shows $\Delta S$ plotted *versus* the $CH_4$ content in the $H_2$–$CH_4$ reduction gas mixture. Similarly to what was observed for $S_n$ (Fig. 5), $\Delta S$ almost linearly increases (up to 7.78 $m^2\ g^{-1}$) with $CH_4$ content increase up to 24 mol% $CH_4$ (region I in Fig. 6). For higher $CH_4$ contents, $\Delta S$ remains constant (*ca.* $7.5 \pm 0.5$) $m^2\ g^{-1}$ (region II in Fig. 6). Thus it appears at this stage that the carbon content is considerably increased [Fig. 4(a)] in specimens R30 and R45 without any enhancement of the quantity of $C_{NTs}$. This could arise owing to the deposition of a strong proportion of non-tubular carbon forms and/or to a thickening of the nanotubes.

The values of $C_n$, $S_n$ and $S_{on}$ measured for the $\alpha$-$Al_2O_3$ powders heat-treated in different $H_2$-$CH_4$ atmospheres are compared with the Fe-containing specimens in Table 3. The

**Table 3** Some characteristics of the powders prepared by $H_2$–$CH_4$ thermal treatment of pure $\alpha$-$Al_2O_3$[a]

| $CH_4$ (mol%) | $C_n$ (wt%) | $S_n$/ $m^2\,g^{-1}$ | $(S_{on})_2$/ $m^2\,g^{-1}$ | $\Delta S$/ $m^2\,g^{-1}$ | $\delta(\Delta S)$/ $m^2\,g^{-1}$ |
|---|---|---|---|---|---|
| 4.5 | 0.46 | 7.05 | 6.50 | 0.55 | 0.41 |
| 12 | 0.55 | 6.98 | 6.50 | 0.48 | 0.40 |
| 18 | 0.95 | 7.18 | 6.50 | 0.68 | 0.41 |
| 24 | 1.67 | 7.02 | 6.50 | 0.52 | 0.41 |

[a]Carbon content ($C_n$) and specific surface areas [$S_n$: value measured for the reduced powders; $S_{on}$: value retained for the calculations corresponding to the powders oxidized at 900 °C; $\Delta S = S_n - S_{on}$, representing the quantity of carbon nanotubes (see text); $\delta(\Delta S)$: uncertainty on $\Delta S$].

carbon content ($C_n$) increases with the increase in the concentration of $CH_4$, whereas $\Delta S$ remains constant and fairly small (*ca.* 0.55 $m^2\,g^{-1}$). This shows that increasing the amount of deposited carbon does not produce an increase in surface area in the absence of catalyst particles. In addition, it should be noted that it was not possible to detect any filamentous form of carbon by SEM observation of these powders. Thus, $\Delta S$ in these powders corresponds to non-tubular carbon species deposited on the alumina grains. In the presence of catalyst particles, it is a reasonable assumption that the amount of such non-tubular carbon is lower, for a given $CH_4$ concentration, and thus that the associated $\Delta S$ is significantly lower than 0.55 $m^2\,g^{-1}$. Comparison with $C_n$ and $\Delta S$ results obtained for the $C_{NTs}$–Fe/$Fe_3C$–$Al_2O_3$ powders (Table 2) confirms the validity of the present characterisation method.

As proposed elsewhere,[16,18] $\Delta S/C_n$ can be considered as a criterion of quality of the carbon, a higher figure for $\Delta S/C_n$ denoting more carbon in tubular form and/or a smaller average tube diameter and/or tubes with fewer walls. Before examining the calculated $\Delta S/C_n$ values, attention should be paid to the calculation of the uncertainties. Indeed, from the relative uncertainty on $S_n$ and $S_{on}$ ($\pm 3\%$), the resulting absolute uncertainties on $\Delta S$ are in the range 0.3–0.5 $m^2\,g^{-1}$ [$\delta(\Delta S)$, Table 2]. Taking into account the accuracy of the carbon analysis ($\pm 2\%$), the resulting absolute uncertainties [$\delta(\Delta S/C_n)$, Table 2] are very high, compared to the $\Delta S/C_n$ values, for specimens R3 and R4.5 ($124 \pm 92$ $m^2\,g^{-1}$ and $172 \pm 47$ $m^2\,g^{-1}$, respectively), which yield relative uncertainties of 69 and 27%, respectively. The evolution of the quality parameter $\Delta S/C_n$ (Fig. 7) *versus* the $CH_4$ content in the reduction gas mixture can be divided into three regions denoted A, B and C. Between 9 and 18 mol% (region B), $\Delta S/C_n$ remains constant (*ca.* 230 $m^2\,g^{-1}$) whereas for higher $CH_4$ contents (region C), it regularly decreases to only 41 $m^2\,g^{-1}$ for 45 mol%. In region A, it is difficult to conclude about the evolution owing to the high uncertainties. However, both the steadiness in the increase of the measured values in region A and the fact that all the measured values of region B are higher than those in region A lead to infer that the increase in region A is significant. It is possible that the uncertainties on the specific surface area measurements are overestimated. Walker *et al.*[39,40] have also reported specific surface areas in the range 35–170 $m^2\,g^{-1}$ for carbon filaments, which they correlate to a high degree of internal porosity because the geometrical surface area of their filaments (100 nm in diameter and 1 mm long) does not exceed 15 $m^2\,g^{-1}$. In contrast, the electron microscopy observations presented below, as well as previous studies,[16,18] have revealed important quantities of very long tubes of nanometric diameter, the geometrical surface area of which is of the order of several hundreds $m^2\,g^{-1}$. Other researchers[15,41,42] have reported increases in specific surface area upon the catalytic formation of carbon nanofibers, which are in qualitative agreement with the present results.

In agreement with earlier studies[18,19] the maximum of the quantity parameter ($\Delta S = 7.78$ $m^2\,g^{-1}$ for R24) is not simultaneously obtained with the maximum of the quality parameter ($\Delta S/C_n = ca.$ 230 $m^2\,g^{-1}$ for R9–R18 compared to $\Delta S/C_n =$ 161 $m^2\,g^{-1}$ for R24), and thus a compromise between quantity and quality must be chosen depending on the envisioned applications. More $C_{NTs}$ are obtained for R24 than in powders R9–R18, but they probably are thicker and/or R24 also contain more non-tubular carbon. For higher $CH_4$ contents, despite a large increase in carbon content [Fig. 4(a)], the quantity and quality simultaneously decrease, which probably reflects the deposition of large quantities of non-tubular carbon. Electron microscopy observations presented in the following sections will help to clarify this point. However, it is noteworthy that the present results are noticeably superior to those previously obtained when also starting from solid solutions in the corundum form.[18,19] Indeed, the specimen with the highest quantity of $C_{NTs}$ previously[18] ($\Delta S =$ 4.9 $m^2\,g^{-1}$) was also one with a fairly poor quality parameter ($\Delta S/C_n = 79$ $m^2\,g^{-1}$); this powder had been prepared by selective reduction of $\alpha$-$Al_{1.8}Fe_{0.2}O_3$ (1000 °C, 4 h, 6 mol% $CH_4$). The composite powder with the highest carbon quality previously[19] ($\Delta S/C_n = 250 \pm 25$ $m^2\,g^{-1}$) was one containing very low $C_{NTs}$ ($\Delta S = 1.8$ $m^2\,g^{-1}$). This powder was prepared by selective reduction of $\alpha$-$Al_{1.9}Fe_{0.1}O_3$ (900 °C, 4 h, 6 mol% $CH_4$), *i.e.* a specimen with a Fe content half that the previous one (highest quantity specimen) and identical to the present powders. Thus it appears that the present powders R9–R18

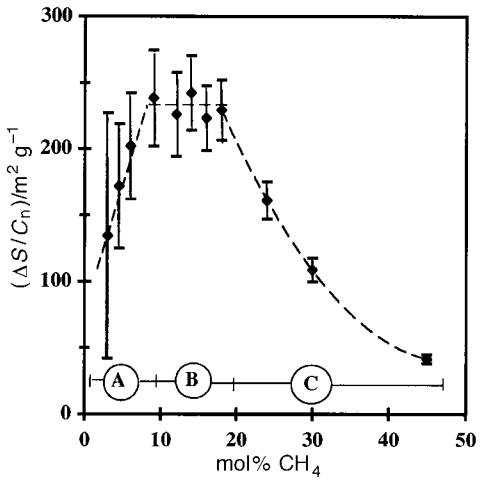


**Fig. 7** $\Delta S/C_n$ *versus* the $CH_4$ content in the $H_2$–$CH_4$ reduction gas mixture.

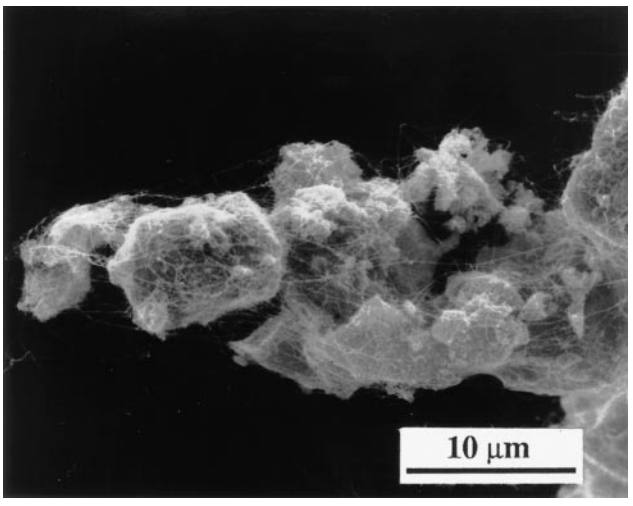


**Fig. 8** SEM image of the nanocomposite powder prepared by reduction in $H_2$–$CH_4$ gas mixtures containing 30 mol% $CH_4$, showing the web of carbon filaments around the matrix grains.

(in region B of Fig. 7) are superior to these two previous specimens. Since the quality of the R9–R18 powders is the same (Fig. 7) and the $C_{NTs}$ quantity increases with the $CH_4$ content (Fig. 6), it may be considered that powder R18 represents the best $C_{NTs}$–Fe–$Al_2O_3$ composite obtained so far ($\Delta S = 6.1\ m^2\ g^{-1}$ and $\Delta S/C_n = 230\ m^2\ g^{-1}$).

**Electron microscopy**

The low-magnification SEM image of the R30 powder (Fig. 8) shows numerous matrix grains, up to 10 μm in size, held together by a web-like network of $C_{NTs}$ bundles. This reflects both the high quantity and the good homogeneity of the dispersion of the $C_{NTs}$ bundles between the matrix grains in this nanocomposite powder. Moreover, this particular microstructure explains why most powders (R6–R45) retain the shape of the reduction vessel when transferred to a storage box. At a higher magnification, some differences appear on the SEM images (Fig. 9) between powders prepared using different $CH_4$ contents. Indeed, we can define three groups of powders that more or less fit with regions A, B and C in the quality data plot (Fig. 7). At lower $CH_4$ contents, few filaments are observed in R4.5 and R6 [Fig. 9(a)] and very few in R1.5 and R3. For intermediate $CH_4$ contents (specimens R9–R18), filaments are clearly observed and are extensively branched in bundles, the diameter of which sometimes reaches 100 nm [Fig. 9(b), (c)]. For higher $CH_4$ contents (R24–R45), it seems that the quantity of filaments has not been increased, but they seem more branched, less straight and the bundles diameter is generally lower than 50 nm [Fig. 9(d)–(f)]. Moreover, for R45 [Fig. 9(f)], numerous heaps, several tens of nanometer in size, are observed at the filament junctions and some spheroidal deposits, 50–100 nm in size, are detected on the matrix grains. These heaps and spheroidal deposits most probably are amorphous and/or crystallized carbon particles. Note that for lower and intermediate $CH_4$ contents ($\leqslant 18$ mol%) such deposits were not observed [Fig. 9(a)–(c)]. Smaller spheroidal species were also observed, at a lower level, at the surface of some matrix grains for R24 [Fig. 9(d)] and at the filament connections for R30 [Fig. 9(e)]. Thus, one may propose that

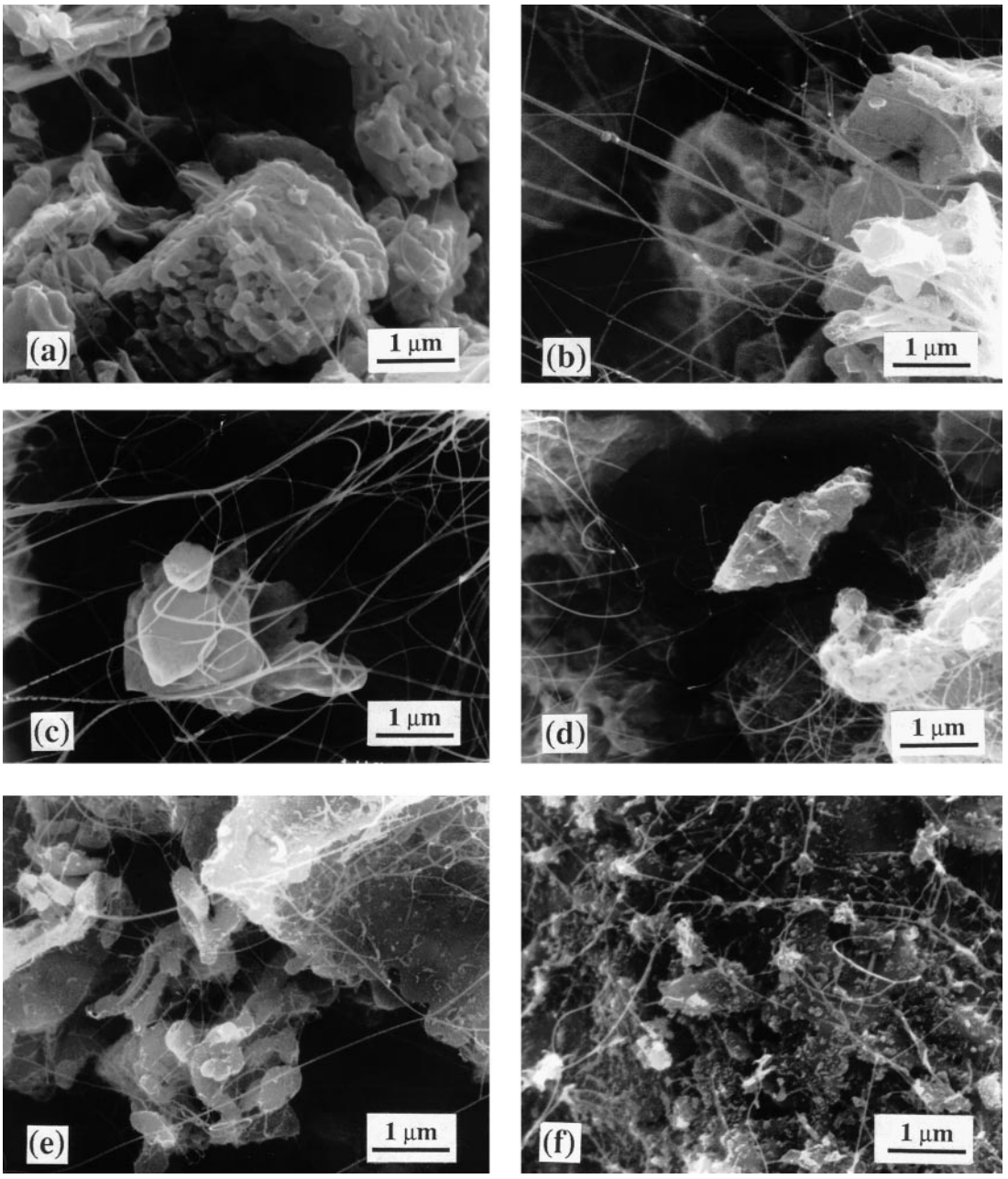


**Fig. 9** SEM images of the nanocomposite powders prepared by reduction in $H_2$–$CH_4$ gas mixtures of different $CH_4$ contents: (a) 6 mol%, (b) 12 mol%, (c) 16 mol%, (d) 24 mol%, (e) 30 mol%, (f) 45 mol%.

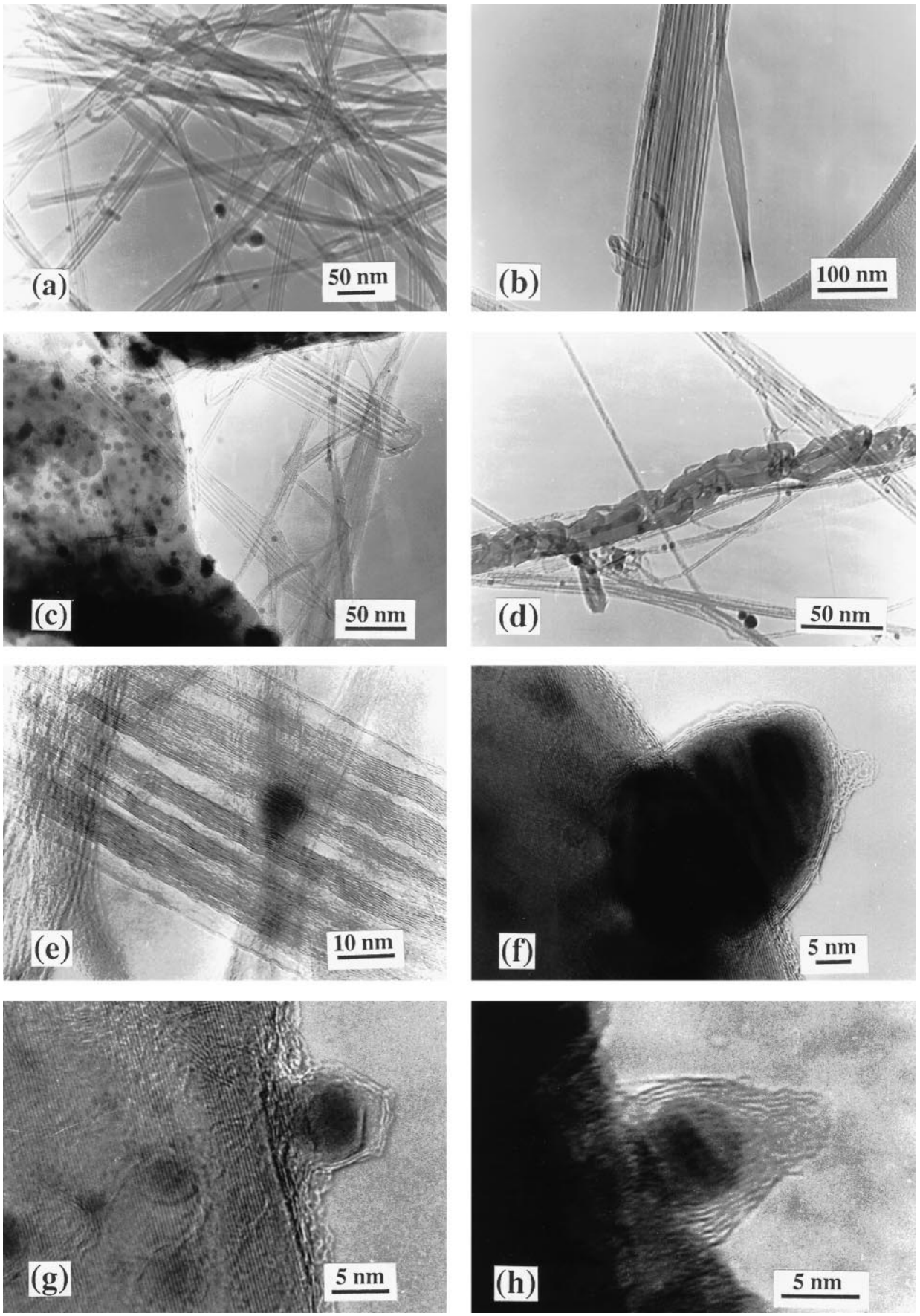


**Fig. 10** TEM (a–d) and HREM (e–h) images of some nanocomposite powders prepared by reduction in $H_2$–$CH_4$ gas mixtures of different $CH_4$ contents: (a) 12 mol%, (b–g) 16 mol%, (h) 18 mol%.

it is the deposition of such non-tubular carbon species, when using a $CH_4$ content higher than 18 mol%, that leads to a strong decrease of the quality parameter for these powders ($\Delta S/C_n = 161$, 109 and 41 $m^2\,g^{-1}$ for R24, R30 and R45, respectively), compared to that calculated for powders prepared with intermediate $CH_4$ contents (*ca.* 230 $m^2\,g^{-1}$).

The R12, R16 and R18 powders were selected for TEM and HREM observations from the results of the above specific surface area studies and SEM observations. Indeed, these composites present both high quantity and high quality parameters and no carbon form other than the filaments is detected by SEM. It should be emphasized that the TEM [Fig. 10(a)–(d)] and HREM [Fig. 10(e)–(h)] images do not reflect a particular characteristic of the powder under examination since similar features have been observed for all three powders. A net of entangled $C_{NTs}$ and $C_{NTs}$ bundles, between 2.5 and 25 nm in outer diameter, is shown in Fig. 10(a). Some catalyst nanoparticles are located at the surface of the tubes, but otherwise the surface appears to be free of amorphous carbon. Also, it seems that no pyrolytic thickening of the tubes has taken place. One of the largest bundles that was observed in the present study (almost 100 nm in diameter) is shown in Fig. 10(b). An isolated nanotube, which appears to be twisted (bottom of the image) is seen to merge with the bundle. The right-hand side of Fig. 10(c) shows bundles of $C_{NTs}$ and some catalyst particles, which seem to be dispersed at the surface of the tubes, rather that included inside, similarly to what is observed in Fig. 10(a). The left-hand side of Fig. 10(c) shows bundles superimposed on a matrix grain. Metal or carbide particles (appearing as dark dots on the image) have a diameter smaller than 10 nm. Previous studies on carbon-free Fe–$Al_2O_3$ nanocomposites[38,43,44] have shown that most of the Fe particles are dispersed within the oxide grains, but that some are located at the surface. It is the latter population of particles which catalyze $CH_4$ decomposition and act as nucleation sites and possibly growth sites for the $C_{NTs}$. An irregularly shaped tube, partially filled with catalyst particles and which seems to have undergone some pyrolytic thickening is shown in Fig. 10(d) together with $C_{NTs}$ bundles. It is emphasized that such a tubular structure, which resembles those reported by several authors working on carbon fibres and filaments (see Rodriguez[45] for a review), is extremely rarely observed in the present composite powders. Important quantities of similar short, thick tubes were also observed in composite powders prepared from an amorphous oxide solid solution,[18] which was found to be an unfavourable starting compound because its relatively high specific surface area notably allows the catalyst particles to grow to a size excessive for the formation of Iijima-type $C_{NTs}$. The interference fringes produced by the graphene layers in a bundle of $C_{NTs}$ almost 50 nm in diameter [Fig. 10(e)] could indicate that the $C_{NTS}$ have a crystallographical organization within the bundle in agreement with reports by other researchers.[46,47] Fig. 10(f) shows a catalyst particle, *ca.* 30 nm in size, located at the surface of a matrix grain and covered by a few graphene layers. Interestingly, there is an amorphous protuberance, about 5 nm in size, located upon the graphene layers. Maiti *et al.*[48] have proposed a model for the nucleation and growth of $C_{NTS}$ when the metal particles are much larger than the tube diameter and researchers using the arc-discharge technique have reported the radial growth of single-walled $C_{NTS}$ from Ni carbide particles[49,50] and from $YC_2$ particles.[51] A much smaller catalyst particle (*ca.* 5 nm) also covered by graphene sheets is shown in Fig. 10(g). The particle is faceted and, most interestingly, there is an empty space between one of the facets (almost vertical on the image) and the corresponding graphene layers. This could indicate that $C_{NTs}$ indeed nucleate on the Fe-based nanoparticles and this could be an image of a nanotube at the very begining of its growth. If so, this would support a closed-end growth mode. In contrast, the protruding, poorly organized, carbon shells surrounding a catalyst particle *ca.* 5 nm in diameter [Fig. 10(h)] could represent the base of a multiwalled nanotube growing with its upper end open.

HREM digital images on individual $C_{NTs}$ observed in powder R12 are shown in Fig. 11. Indeed, since the electron beam very often induces vibrations and sometimes a deterioration of the tubes, the instantaneous capture of digital images from a camera was found to be the most efficient way to observe resolved (002) planes within the multiwalled nanotubes. A nanotube of 4.3 nm diameter is shown in Fig. 11(a). It is not possible to conclude, using this magnification, whether the

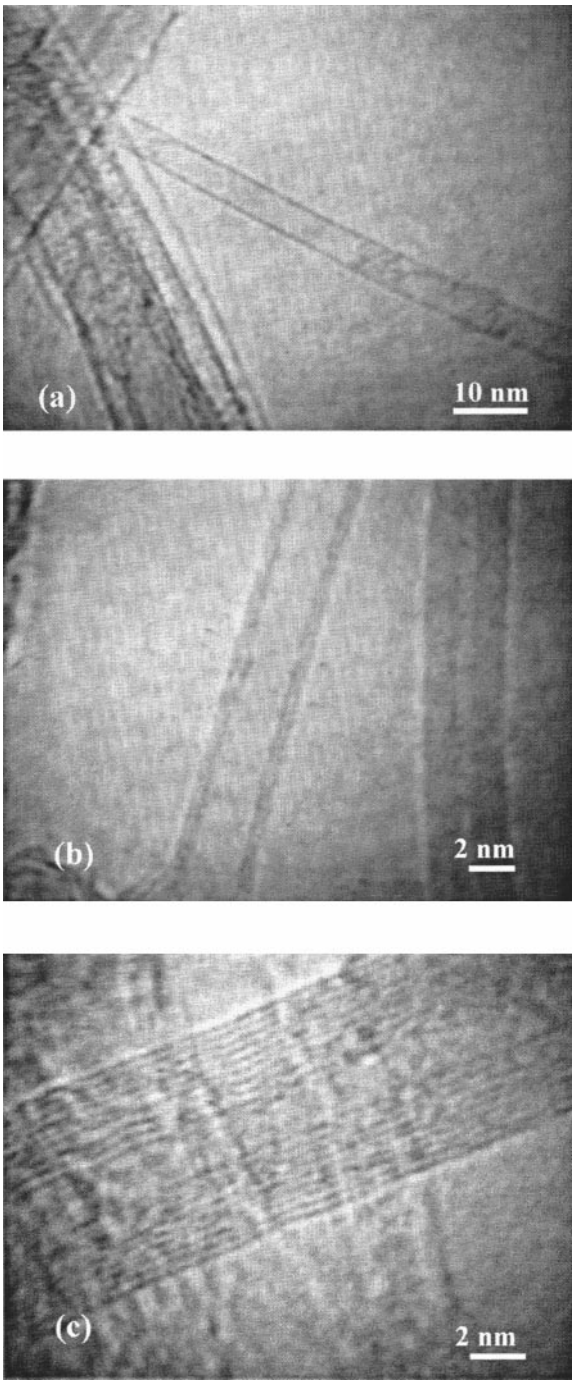


**Fig. 11** HREM digital images of the nanocomposite powder prepared by reduction in $H_2$–$CH_4$ gas mixtures containing 12 mol% $CH_4$, showing (a) a single or two-walled nanotube 4.3 nm in diameter, (b) two-walled nanotube with an outer diameter equal to 3 nm and (c) a nine-walled nanotube with an outer diameter equal to 7.8 nm. Note that almost all the $C_{NTs}$ observed in HREM were free of pyrolytic or amorphous carbon deposits and have an inner diameter in the range 1–6 nm.

nanotube is a single- or two-walled tube. Some single-wall nanotubes were observed in this specimen but often rapidly deteriorated under the electron beam. A two-walled nanotube with an outer diameter equal to 3 nm is shown in Fig. 11(b) and a nine-walled nanotube with an outer diameter equal to 7.8 nm is shown in Fig. 11(c). Almost all the $C_{NTs}$ observed in HREM were free of pyrolytic or amorphous carbon deposits and have an inner diameter in the range 1–6 nm. This could indicate that the catalyst particles active for $C_{NTs}$ formation are in this size range. Very few multi-walled nanotubes had more than 10 walls, most having two, three or four walled.

#### Influence of the $CH_4$ content in the $H_2$–$CH_4$ atmosphere

The above results obtained on both a macroscopic and a microscopic scale show that the $CH_4$ content in the $H_2$–$CH_4$ atmosphere is a key parameter for the formation of Iijima-type $C_{NTs}$ preferentially to other carbon species. The amount of carbon deposited in the composite powder continuously increases with an increase in $CH_4$ concentration, whereas the quantity of $C_{NTs}$ is maximum for 24 mol% $CH_4$ and the carbon quality is maximum for the range 9–18 mol% $CH_4$. For specimens prepared using a $CH_4$ content lower than 9 mol% (A powders), the amount of deposited carbon is low ($\leqslant$1%) and the quantity of nanotubes is accordingly low. However, by contrast to what might have been expected from earlier studies,[18,19] it is not these powders for which the carbon quality is maximal. This could reflect that carbon is preferentially engaged in species such as Fe–C alloys, $Fe_3C$ and graphenic layers at the surface of the catalyst particles, rather than in $C_{NTs}$. However, the increase in both quantity and quality when the $CH_4$ content is changed from 1.5 to 6 mol% indicates that the proportion of carbon engaged in $C_{NTs}$ increases. For composite powders prepared using $H_2$–$CH_4$ gas mixtures containing between 9 and 18 mol% $CH_4$ (B powders), the quantity of $C_{NTs}$ steadily increases with the $CH_4$ content with the quality of carbon being constant. This could indicate that the extra $CH_4$ content in the atmosphere produces carbon that is contributing solely to the formation of $C_{NTs}$ and that the maximum quality achievable in the present experimental condition is obtained. By contrast, for specimens prepared using a $CH_4$ content higher than 18 mol% (C powders), the quantity of $C_{NTs}$ is constant and there is a decrease in the quality parameter upon the increase in $CH_4$ content. This is mainly due to the formation of non-tubular carbon species, mostly spheroidal carbon particles, which could reflect a very high carbon deposition rate.

The proposition that differences in the reduction rate (reflected by the proportion of $Fe^{3+}$ ions remaining in the oxide matrix) depending on the $CH_4$ content in the reducing atmosphere may influence the formation of $C_{NTs}$ through modifications of the quantity and size of the catalyst particles formed at the surface of the matrix grains can be ruled out for the following reasons: it appears that the reducing power of the $H_2$–$CH_4$ atmosphere decreases with increase in $CH_4$ content above 1.5 mol% and that differences in reduction rate only modify the proportion of nanoparticles which are inactive because they are located inside the matrix grains.

The considerable debate on the nature of the catalytic phase responsible for the formation of filamentous carbon has been reviewed by Rodriguez.[45] In particular, Baker *et al.*[52] claimed that $Fe_3C$ particles supported on graphite and exposed to acetylene were not catalytic for the formation of carbon nanofilaments. In contrast, Sacco *et al.*[53] claimed that $Fe_3C$ acts as a catalyst for CO decomposition, carbon deposition and subsequent filament growth. However, the formation of Iijima-type $C_{NTs}$ involves much smaller catalyst particles, as pointed out above, and the mechanisms for their nucleation and growth are different from those proposed in the case of hollow filaments. The present study does not allow us to conclude on the catalytic role of α-Fe, Fe–C alloy and $Fe_3C$, but it is clear that the detection of $Fe_3C$ by post-reaction Mössbauer spectroscopy analysis is not to be considered as an indication of poor quality results. However, the propensity of carbon to form a carbide phase in the presence of Fe means that it is inevitable that a fraction of the carbon provided by the gas phase is lost for the formation of $C_{NTs}$. Thus better results may be achieved by using, for example, Co or Fe/Co alloy particles as catalysts.[21,22] Interestingly, carbide phases were not detected in such $C_{NTs}$–Co–$MgAl_2O_4$ and $C_{NTs}$–Fe/Co–$MgAl_2O_4$ powders,[21,22] but is is noteworthy that Ivanov *et al.*[14] claimed that a Co carbide and not Co is the active catalyst for the production of $C_{NTs}$ from a zeolite-supported Co catalyst. This point is obviously not settled and underlines the need for future studies.

## Conclusions

$C_{NTs}$–Fe/$Fe_3C$–$Al_2O_3$ nanocomposite powders have been prepared by selective reduction of a monophase α-$Al_{1.9}Fe_{0.1}O_3$ solid solution in different $H_2$–$CH_4$ gas mixtures (0, 1.5, 3, 4.5, 6, 9, 12, 14, 16, 18, 24, 30 and 45 mol% $CH_4$). The powders have been studied using a combination of chemical analysis, X-ray diffraction, Mössbauer spectroscopy, scanning and transmission electron microscopy and specific surface area measurements. We have notably made use of a method (chemical analysis) and specific surface area measurements allowing characterization of the composite powders at a macroscopical scale, thus producing results more representative of the material than do local techniques.

It has been shown that the reduction of the $Fe^{3+}$ ions to metallic Fe is highly favoured by the presence of $CH_4$ in the reduction atmosphere, notably at low $CH_4$ contents. However, the subsequent differences between powders seem to mainly concern intragranular particles inactive for the formation of $C_{NTs}$. α-Fe and $Fe_3C$ particles located at the surface of the matrix grains represent *ca.* 26% of all the iron species whatever the $CH_4$ content and no clear evolution of their respective proportion could be observed. The trend is that there is more $Fe_3C$ than α-Fe for $CH_4$ contents higher than 4.5 mol%.

More carbon is deposited when the $CH_4$ concentration is increased, whereas the quantity of $C_{NTs}$ is maximum for 24 mol% $CH_4$ and the carbon quality is maximum for the range 9–18 mol% $CH_4$. For specimens prepared using a $CH_4$ content lower than 9 mol%, it is proposed that carbon is preferentially engaged in species such as Fe–C alloys, $Fe_3C$ and graphenic layers at the surface of the catalyst particles rather than in $C_{NTs}$. However, the proportion of $C_{NTs}$ increases with an increase in $CH_4$ content. For $CH_4$ concentrations ranging between 9 and 18 mol%, it is proposed that the extra $CH_4$ content in the atmosphere produces carbon solely contributing to the formation of $C_{NTs}$ and that the maximum quality achievable in the present experimental condition is obtained in this range. For higher $CH_4$ contents, the quantity of $C_{NTs}$ is constant and formation of spheroidal carbon particles causes a decrease in quality.

The $C_{NTs}$ are arranged in very long bundles homogeneously dispersed in the composite powder. Most $C_{NTs}$ have two, three or four walls. Single-walled tubes have also been observed. Almost all the $C_{NTs}$ observed in HREM are free of pyrolytic or amorphous carbon deposits and have an inner diameter in the range 1–6 nm, which could indicate that the catalyst particles active for $C_{NTs}$ formation are in this size range. The exact nature of these particles remains an open question.

## Acknowledgements

The authors would like to thank Mr. L. Datas for his assistance in the TEM and HREM observations.

## References


1 S. Iijima, *Nature* (*London*), 1991, **354**, 56.
2 S. B. Sinnott, C. T. White and D. W. Brenner, *Mater. Res. Soc. Symp. Proc.*, 1995, **359**, 241.
3 J. F. Despres, E. Daguerre and K. Lafdi, *Carbon*, 1995, **33**, 87.
4 M. M. J. Treacy, T. W. Ebbesen and J. M. Gibson, *Nature* (*London*), 1996, **381**, 678.
5 S. Iijima, C. Brabec, A. Maiti and J. Bernholc, *J. Chem. Phys.*, 1996, **104**, 2089.
6 B. I. Yakobson, C. J. Brabec and J. Bernholc, *Phys. Rev. Lett.*, 1996, **76**, 2511.
7 M. R. Falvo, G. J. Clary, R. M. Taylor III, V. Chi, F. P. Brooks, Jr., S. Washburn and R. Superfine, *Nature* (*London*), 1997, **389**, 582.
8 J. P. Lu, *J. Phys. Chem. Solids*, 1997, **58**, 1649.
9 P. Calvert, *Nature* (*London*), 1992, **357**, 365.
10 P. M. Ajayan, O. Stephan, C. Colliex and D. Trauth, *Science*, 1994, **265**, 1212.
11 R. S. Ruoff and D. C. Lorents, *Carbon*, 1995, **33**, 925.
12 C. Journet and P. Bernier, *Appl. Phys. A*, 1998, **67**, 1.
13 Ch. Laurent, E. Flahaut, A. Peigney and A. Rousset, *New J. Chem.*, 1998, **22**, 1229.
14 V. Ivanov, A. Fonseca, J. B. Nagy, A. Lucas, P. Lambin, D. Bernaerts and X. B. Zhang, *Carbon*, 1995, **33**, 1727.
15 K. Hernadi, A. Fonseca, J. B. Nagy, D. Bernaerts, A. Fudala and A. A. Lucas, *Zeolites*, 1996, **17**, 416.
16 A. Peigney, Ch. Laurent, F. Dobigeon and A. Rousset, *J. Mater. Res.*, 1997, **12**, 613.
17 Ch. Laurent, A. Peigney, F. Dumortier and A. Rousset, *J. Eur. Ceram. Soc.*, 1998, **18**, 1995.
18 Ch. Laurent, A. Peigney and A. Rousset, *J. Mater. Chem.*, 1998, **8**, 1263.
19 A. Peigney, Ch. Laurent, F. Dumortier and A. Rousset, *J. Eur. Ceram. Soc.*, 1998, **18**, 2005.
20 D. D. Wagmann, J. E. Kirpatrick, W. J. Taylor, K. S. Pitzer and F. D. Rossini, *J. Res. Natl. Bur. Stand.,* 1945, **34**, 143.
21 A. Govindaraj, E. Flahaut, Ch. Laurent, A. Peigney, A. Rousset and C. N. R. Rao, *J. Mater. Res.*, 1999, submitted.
22 E. Flahaut, A. Govindaraj, A. Peigney, Ch. Laurent, A. Rousset and C. N. R. Rao, *Chem. Phys. Lett.*, 1999, **300**, 236.
23 Ch. Laurent, A. Rousset, M. Verelst, K. R. Kannan, A. R. Raju and C. N. R. Rao, *J. Mater. Chem.*, 1993, **3**, 513.
24 G. G. Tibbetts, M. G. Devour and E. J. Rodda, *Carbon*, 1987, **25**, 367.
25 G. A. Jablonski, F. W. Geurts, A. Sacco, Jr. and R. R. Biederman, *Carbon*, 1992, **30**, 87.
26 F. Benissad-Aissani and P. Gadelle, *Carbon*, 1993, **31**, 21.
27 S. Cui, Y. L. Tian, C. Z. Lu, H. M. Kang, Y. L. Qiao and L. Cui, in *Extended Abstracts*, *Eurocarbon'98*, Strasbourg, France, 1998, p. 869.
28 K. Hernadi, A. Fonseca, J. B. Nagy, D. Bernaerts and A. Lucas, *Carbon*, 1996, **34**, 1249.
29 J. Kong, A. M. Cassell and H. Dai, *Chem. Phys. Lett.*, 1998, **292**, 567.
30 X. Devaux, Ch. Laurent and A. Rousset, *NanoStruct. Mater.*, 1993, **2**, 339.
31 H. L. Yakel, *Int. Met. Rev.*, 1985, **30**, 17.
32 G. Le Caër, J. M. Dubois and J. P. Sénateur, *J. Solid State Chem.*, 1976, **19**, 19.
33 X. X. Bi, B. Ganguly, G. P. Huffman, F. E. Huggins, M. Endo and P. C. Eklund, *J. Mater. Res.*, 1993, **8**, 1666.
34 H. Ino, T. Moriya, F. E. Fujita, Y. Maeda, Y. Ono and Y. Inokuti, *J. Phys. Soc. Jpn.*, 1968, **25**, 88.
35 E. Bauer-Grosse, G. Le Caër and L. Fournes, *Hyperfine Interact.*, 1986, **27**, 297.
36 O. Quénard, E. De Grave, Ch. Laurent and A. Rousset, *J. Mater. Chem.*, 1997, **7**, 2457.
37 M. Verelst, K. R. Kannan, G. N. Subbanna, C. N. R. Rao, Ch. Laurent and A. Rousset, *J. Mater. Res.*, 1992, **7**, 3072.
38 A. Marchand, X. Devaux, B. Barbara, P. Mollard, M. Brieu and A. Rousset, *J. Mater. Sci.*, 1993, **28**, 2217.
39 P. L. Walker, Jr., J. F. Rakszawski and G. R. Imperial, *J. Phys. Chem.,* 1959, **63**, 133.
40 P. L. Walker, Jr., J. F. Rakszawski and G. R. Imperial, *J. Phys. Chem.*, 1959, **63**, 140.
41 N. M. Rodriguez, M.-S. Kim and R. T. K. Baker, *J. Phys. Chem.*, 1994, **98**, 13108.
42 W. B. Downs and R. T. K. Baker, *J. Mater. Res.*, 1995, **10**, 625.
43 X. Devaux, Ch. Laurent, M. Brieu and A. Rousset, *J. Alloys Compd.*, 1992, **188**, 179.
44 Ch. Laurent, Ch. Blaszczyk, M. Brieu and A. Rousset, *NanoStruct. Mater.*, 1995, **6**, 317.
45 N. M. Rodriguez, *J. Mater. Res.*, 1993, **8**, 3233.
46 A. Thess, R. Lee, P. Nikolaev, H. Dai, P. Petit, J. Robert, D. T. Colbert, C. Xu, Y. H. Lee, S. G. Kim, A. G. Rinzler, G. E. Scuseria, D. Tomanek, J. E. Fisher and R. E. Smalley, *Science*, 1996, **273**, 483.
47 C. Journet, W. K. Maser, P. Bernier, A. Loiseau, M. Lamy de la Chapelle, S. Lefrant, P. Deniard, R. Lee and J. E. Fisher, *Nature* (*London*), 1997, **388**, 756.
48 A. Maiti, C. J. Brabec and J. Bernholc, *Phys. Rev. B*, 1997, **55**, 6097.
49 Y. Saito, M. Okuda, N. Fujimoto, T. Yoshikawa, M. Tomita and T. Hayashi, *Jpn. J. Appl. Phys. 2*, 1994, **33**, L526.
50 Y. Saito, *Carbon*, 1995, **33**, 979.
51 D. Zhou, S. Seraphin and S. Wang, *Mater. Res. Soc. Symp. Proc.*, 1994, **349**, 257.
52 R. T. K. Baker, J. R. Alonzo, J. A. Dumesic and D. J. C. Yates, *J. Catal.*, 1977, **74**, 82.
53 A. Sacco, Jr., P. Thacker, T. N. Chang and A. T. S. Chiang, *J. Catal.*, 1984, **85**, 224.


*Paper 8/09114E*